A Paradigm for Enzyme-Catalyzed Proton Transfer at Carbon: Triosephosphate Isomerase

ARTICLE *in* BIOCHEMISTRY · MARCH 2012

Impact Factor: 3.02 · DOI: 10.1021/bi300195b · Source: PubMed

1 AUTHOR:

John P. Richard
University at Buffalo, The State University of …

219 PUBLICATIONS **6,855** CITATIONS

SEE PROFILE

Published in final edited form as:
Biochemistry. 2012 April 3; 51(13): 2652–2661. doi:10.1021/bi300195b.

A Paradigm for Enzyme-Catalyzed Proton Transfer at Carbon: Triosephosphate Isomerase

John P. Richard[*,†]
Department of Chemistry, University at Buffalo, SUNY, Buffalo, New York 14260-3000

Abstract

Triosephosphate isomerase (TIM) catalyzes the stereospecific 1,2-proton shift at dihydroxyacetone phosphate (DHAP) to give (*R*)-glyceraldehyde 3-phosphate through a pair of isomeric enzyme-bound *cis*-enediolate phosphate intermediates. The chemical transformations that occur at the active site of TIM were well understood by the early 1990s. The mechanism for enzyme-catalyzed isomerization is similar to that for the nonenzymatic reaction in water, but the origin of the catalytic rate acceleration is not understood. We review the results of experimental work which show that a substantial fraction of the large 12 kcal/mol intrinsic binding energy of the non-reacting phosphodianion fragment of TIM is utilized to activate the active site side chains for catalysis of proton transfer. Evidence is presented that this activation is due to a phosphodianion driven conformational change, the most dramatic feature of which is closure of loop 6 over the dianion. The kinetic data are interpreted within the framework of a model where activation is due to the stabilization by the phosphodianion of a rare, desolvated, loop closed form of TIM. The dianion binding energy is proposed to drive the otherwise thermodynamically unfavorable desolvation of the solvent-exposed active site. This reduces the effective local dielectric constant of the active site, in order to enhance stabilizing electrostatic interactions between polar groups and the anionic transition state; and, increases the basicity of the carboxylate side chain of Glu-165 that functions to deprotonate the bound carbon acid substrate. A rebuttal is presented to the recent proposal [Samanta, M., Murthy, M. R. N., Balaram, H., and Balaram, P. (2011) *Chembiochem 12*, 1886–1895] that the cationic side chain of K12 functions as an active site electrophile to protonate the carbonyl oxygen of DHAP.

The contradiction between the perception that X-ray crystal structures of enzymes place in plain view everything needed to explain their catalytic rate acceleration, and the reality that there are substantial gaps in our understanding of enzyme catalysis is apparent when considering the complex problem of designing proteins with enzymatic activity (1). We need to improve our understanding of the explanation for enzymatic rate accelerations and the best way to move forward is to focus on enzymes whose mechanisms are already well understood.

Triosephosphate isomerase (TIM)[1] catalyzes the stereospecific 1,2-proton shift at dihydroxyacetone phosphate (DHAP) to give (*R*)-glyceraldehyde 3-phosphate through a pair of isomeric enzyme-bound *cis*-enediolate phosphate reaction intermediates (Scheme 1) (2).

[*]Tel: (716) 645 4232, Fax: (716) 645 6963, jrichard@buffalo.edu.
[†]This work was supported by Grant GM39754 from the National Institutes of Health

[1]Abbreviations: TIM, triosephosphate isomerase; *Tbb*TIM, TIM from *Trypanosoma brucei brucei; c*TIM, TIM from chicken muscle; monoTIM, engineered monomeric variant of *Tbb*TIM; LDM, loop deletion mutant of TIM; XI, xylose isomerase; DHAP, dihydroxyacetone phosphate; *d*-DHAP, [1(*R*)-^{2}H]-dihydroxyacetone phosphate; GAP, (*R*)-glyceraldehyde 3-phosphate; *d*-GAP, [2(*R*)-^{2}H]-glyceraldehyde 3-phosphate; DGA, D-glyceraldehyde; GA, glycolaldehyde; NMR, nuclear magnetic resonance; NADH, nicotinamide adenine dinucleotide, reduced form; NAD, nicotinamide adenine dinucleotide, oxidized form; PGH, 2-phosphoglycolohydroxamate; PGA, 2-phosphoglycolate.

The enzyme's high cellular abundance (3), low molecular weight (dimer of 26 kDa/subunit), prominent role in the 4 billion year old glycolytic pathway (4) and the centrality of proton transfer reactions at carbon (5) in metabolism (6) have made TIM a prominent target for mechanistic studies (2, 7, 8). Jeremy Knowles and Greg Petsko established a fruitful collaboration through the 1980s and into the 1990s that combined X-ray crystallography with emerging technology for the preparation of site directed mutant enzymes. An important result of this work was to establish the chemical mechanism for isomerization at the enzyme active site (Figure 1). Catalysis proceeds by deprotonation of the enzyme-bound substrate using the carboxylate side chain of Glu-165[2] (9, 10) in a reaction assisted by the neutral imidazole side chain of His-95 (11). The alkylammonium side chain of Lys-12 was shown to play an important, but poorly defined role in providing electrostatic stabilization of the bound substrate dianion (12, 13). A pair of elegant and optimistic reviews (14, 15) from 1991 summarized the many aspects of the reaction mechanism that were well understood, while explaining problems that required additional study.

Only 40 years ago there was a sense of mystery attached to the mechanism of enzyme catalysis, and excitement as X-ray crystal structures exposed the interiors of these catalytic black boxes. The collaborative studies of Knowles and Petsko on TIM had an uplifting influence on myself and other mechanistic enzymologists. However, the chemical reaction mechanism for TIM (Figure 1) is not significantly different from that for nonenzymatic isomerization in water (16). The detailed active site structures provide limited guidance for catalyst design, beyond proposals that catalytic side chains should be tethered at a binding pocket, which is complementary to substrate. However, these side chains must in some sense be activated for catalysis at the enzyme active site compared to water and there is no general agreement about the mechanisms for this activation. We summarize here our mechanistic studies on this problem of enzyme activation.

TIM-Catalyzed Hydron Transfer

The partitioning of tracer levels of tritium in the solvent water and at the substrate [1-(*R*)-^{3}H]-DHAP was monitored in transformative studies to define the relative barriers to the microscopic steps for TIM-catalyzed isomerization (7). We showed many years later that high-resolution ^{1}H NMR spectroscopy is a powerful analytical method for monitoring nonenzymatic proton transfer reactions at carbon in D_2O (17–22). This technique is well suited for studies on the mechanism of action of TIM. It has the advantage over studies with tritium of providing directly the yields of the products of hydron transfer, without the requirement for separation of the labeled hydron in products from that in unreacted substrate.

We have examined TIM-catalyzed deprotonation of GAP (23) or DHAP (24) in D_2O. These reactions proceed through isomeric enediolate intermediates that partition between intramolecular transfer of ^{1}H to product and irreversible exchange of the ^{1}H-labeled enzyme with deuterium from solvent to give ^{2}H-labeled enzyme which, in turn, partitions to form *d*-GAP and *d*-DHAP (Figure 2). The product yields summarized in Figure 2 provided support for several important conclusions from earlier work with tritium at tracer levels in solvent or [1-(*R*)-^{3}H]-DHAP, but raised questions about the following simplifying assumptions made in interpreting these earlier results (23, 24).

1. Hydron transfer between bulk solvent and TIM was assumed to be fast relative to turnover, so that the ^{1}H- and ^{3}H-labeled carboxylic acid side chain of Glu-165 "*are essentially at equilibrium*" (7). Exchange of ^{3}H is fast relative to turnover, as

[2]The numbering is for the sequence of TIM from chicken muscle, unless indicated otherwise.

shown by the nearly complete (≈ 95%) wash out of tritium during the irreversible conversion of [1-(R)-^{3}H]DHAP to GAP in H_2O. TIM-catalyzed isomerization of [2-(*R*)-^{3}H]-GAP was not examined in these earlier studies. Our observation that the TIM-catalyzed reaction of GAP in D_2O gives a 50% yield of DHAP from a reaction with intramolecular transfer of hydrogen (23) shows that $k_{ex} \approx (k_{C1})_H$ (Figure 2). Transfer of ^{1}H from TIM to solvent D_2O (k_{ex}) is therefore too slow relative to turnover to allow the H- and D-labeled enzymes to approach equilibrium with solvent (23).

2. The direct transfer of tritium from TIM to solvent was preferred over the initial transfer of the tritium label to a pool of hydrons at the enzyme active site (25). However, if hydron transfer were directly to solvent, then hydron exchange between enzyme and solvent should be accelerated by general bases such as imidazole (26), as has been well documented for carbonic anhydrase (27). The constant 50% yield of hydrogen labeled product DHAP from the reaction of GAP in D_2O observed as the concentration of the basic form of imidazole buffer is increased from 0.014 to 0.56 M, shows that there is no detectable buffer catalysis of the hydron exchange reaction with solvent (28). Irwin Rose has provided evidence that hydron exchange is initially between the labeled acid and a pool of solvent water molecules at the enzyme active site; and, that the final exchange reaction with bulk solvent occurs after dissociation of product (29).

3. The simplifying assumption was made that isomerization proceeds through a single reaction intermediate (30). This requires either enzyme-catalyzed isomerization of GAP and DHAP through a common enediol phosphate, or that proton transfer between O-1 and O-2 of isomeric enediolate phosphate oxyanions (Figure 2) is fast relative to turnover, so that these anions are effectively at chemical equilibrium. However, we observe different product distributions from the partitioning of the intermediates generated from the TIM-catalyzed reactions of GAP [red products, Figure 2) and of DHAP in D_2O (blue products) (23, 24). This requires different relative steady-state concentrations for the isomeric enediolate phosphate intermediates (Figure 2) during turnover of DHAP and GAP, in which case they cannot be at chemical equilibrium.

The above simplifying assumptions are consistent with a solvent-exposed enzyme active site. They could be partly justified by the seemingly logical, but misguided, notion that there was no clear imperative for sequestering polar substrates at TIM from the polar solvent water, because water already provides strong stabilization of the transition states for polar reactions. Later X-ray crystallographic analyses showed that TIM binds substrate and other ligands at a solvent-exposed cavity, and that binding is followed by closure of loop 6 (residues 166–176, Scheme 2) over the phosphodianion, which *sequesters* the carbon-acid from solvent (31–33). It is now understood that enzymatic catalysis of proton transfer at carbon is favored at solvent-occluded active sites, because of the enhancement of electrostatic interactions between charged transition states and polar side chains that occurs as the local active site dielectric constant is decreased below that for water (34, 35). This includes the strengthening of simple electrostatic interactions along with the tightening of hydrogen bonds, which may take on the structure of low-barrier hydrogen bonds (36, 37).

Phosphodianion binding energy

Pompliano and Knowles reasoned that deletion of residues 170–173 (green in Scheme 2 Figure 3A) of loop 6 and the introduction of a peptide bond between A169 and K174 should disrupt loop-dianion interactions without significantly affecting the protein fold (Figure 3B). The large 10^5-decrease in k_{cat}, and much smaller 2.3-fold increase in K_m determined for

isomerization of GAP catalyzed by the loop deletion mutant (LDM) of TIM from chicken muscle (*c*TIM) provide strong evidence that the benefits of loop-6 closure far exceed any energetic costs, as suggested in by Wolfenden in 1974 (38).

The low catalytic activity of the LDM showed that interactions between the substrate and phosphodianion gripper loop 6 activate TIM for catalysis. This raises the question of the total contribution of protein-phosphodianion interactions to the enzymatic rate acceleration. Truncation of the dianion results in a large falloff in activity from $k_{cat}/K_m = 10^8\ M^{-1}\ s^{-1}$ for TIM-catalyzed isomerization of GAP (39) to $k_{cat}/K_m = 0.34$ (40) and $0.1\ M^{-1}\ s^{-1}$ (41), respectively for the TIM-catalyzed reactions of D-glyceraldehdye (DGA) and [1-^{13}C]-glycolaldehyde ([1-^{13}C]-GA) in D_2O. A 12 kcal/mol intrinsic phosphodianion binding energy was calculated from the falloff in k_{cat}/K_m for the whole compared to truncated substrates (40). TIM-catalyzed deprotonation of DGA is only marginally faster than deprotonation catalyzed by the small general base catalyst 3-quinuclidinone ($k_B = 6.5 \times 10^{-3}\ M^{-1}\ s^{-1}$) (40) so that ca 80% of the transition state stabilization of this near-perfect enzyme is eliminated by truncation of the remote substrate phosphodianion group (40). This is a profoundly significant result, because it shows that the characterization of the enzyme-phosphodianion interactions is central to the development of an understanding of the enzymatic rate acceleration.

A critical question is whether the TIM-phosphodianion interactions simply anchor GAP and DHAP to the enzyme, or if they also activate TIM for catalysis of proton transfer. Cutting the connection between the carbon acid and phosphodianion allows the effect of the dianion interaction to be determined absent this anchor. A very large increase in $(k_{cat}/K_m)_{obs}$ for TIM-catalyzed deuterium exchange reactions of GA in D_2O was observed as the concentration of phosphite dianion was increased (Scheme 3) (42). The yields of the three products of HPO_3^{2-}-activated TIM-catalyzed reactions of [1-^{13}C]-GA in D_2O (Scheme 4) are similar to the yields of the corresponding products of the reactions of the whole substrates (Figure 2) (41). The principal difference between the catalyzed reactions of the whole substrate and its pieces (41–43) is the *ca* 6 kcal/mole entropic advantage provided by connecting the pieces (44). This connection allows triosephosphates to bind and react with the loss of translational and rotational entropy of a single molecule, compared to the larger loss in entropy associated for the binding of the separate pieces GA and HPO_3^{2-} (45).

An analysis of the dependence of $(k_{cat}/K_m)_{obs}$ for rabbit muscle TIM-catalyzed reactions of GA in D_2O on $[HPO_3^{2-}]$ provided three kinetic parameters (Scheme 5); $(k_{cat}/K_m)_E \approx 0.1\ M^{-1}\ s^{-1}$,[3] $K_d = 38$ mM for binding of phosphite dianion and $(k_{cat}/K_m)_{E•Pi} \approx 185\ M^{-1}\ s^{-1}$ (42). Similar kinetic parameters were determined for the reaction catalyzed by TIM from *Trypanosoma brucei brucei* (*Tbb*TIM) (43). The observed interaction between TIM and phosphite dianion is relatively weak ($\Delta G_{obsd} = RT \ln(0.038) = -1.9$ kcal/mole). The 1850-fold larger value of k_{cat}/K_m for catalysis of deprotonation of GA by free enzyme E compared to E•P_i shows that these interactions strengthen to −6.4 kcal/mol ($K_d^{\dagger} \approx 20\ \mu M$, Scheme 5) at the transition state complex E•$GA^{\dagger}$•P_i.

An engineered monomeric variant of *Tbb*TIM (monoTIM) (46) catalyzes isomerization of GAP with $k_{cat}/K_m = 1000\ M^{-1}\ s^{-1}$ (43) that is similar to k_{cat}/K_m for isomerization of xylose catalyzed by xylose isomerase (XI) (47), but much smaller than $k_{cat}/K_m = 10^7\ M^{-1}\ s^{-1}$ for wildtype *Tbb*TIM (43). MonoTIM shows no detectable phosphite activation (43). Apparently, *respectable* catalysis of isomerization of GAP is possible for the monomeric

[3]This is smaller than an earlier published value of $0.26\ M^{-1}\ s^{-1}$ (41), which did not include the complete correction for a competing nonspecific deuterium exchange reaction that occurs outside the active site of TIM (39).

enzyme, but phosphite dianion activation is critical to achieving perfection in catalysis of the isomerization reaction (7).

We have examined 3 enzymes that utilize a phosphodianion gripper loop: TIM, orotidine 5′-monophosphate decarboxylase (48), and α-glycerol phosphate dehydrogenase (49). In each case: (a) A total intrinsic phosphodianion binding energy of 12 kcal/mol was determined from the ratio of second order rate constants k_{cat}/K_m for the enzyme-catalyzed reactions of whole and dianion-truncated substrates. (b) Roughly one-half of this binding energy was observed in phosphite dianion activation of the enzyme-catalyzed reactions of the respective truncated substrates. The striking similarity of these results for enzymes that utilize phosphodianion gripper loops in catalysis of proton transfer, hydride transfer and decarboxylation reactions of phosphorylated substrates is consistent with the notion that a common general mechanism has evolved for using dianion binding interactions to activate enzymes for catalysis.

Phosphodianion binding interactions

The X-ray crystal structure of the complex between TIM and the intermediate analog PGH (50) shows that the 12 kcal/mol intrinsic phosphodianion binding energy is due partly or entirely to hydrogen bonding interactions of the phosphodianion with the backbone amides of Gly-171 (loop 6), Ser-211 (loop 7), Gly-232 and 233 (loop 8) and to an ionic interaction with the cationic side chain of Lys-12. Loop 6 and the side chain K12 lie next to one another on the protein surface (Figure 3A). In addition to the isomerization reaction, the LDM (32) and K12G mutant (51) of TIM catalyze the elimination reaction of triosephosphates to form methylglyoxal and phosphate. Therefore, loop 6, and the cationic side chain of K12 operate in concert to slow the otherwise fast breakdown of the O-1 oxyanion enediolate phosphate intermediate (16, 52).

It is difficult to account for the large 6×10^5-fold effect of the K12G mutation on k_{cat}/K_m (53) by the loss of an ion-pairing interaction of the cationic side chain of K12, and even harder to account for the 10^5-fold effect of the LDM (Figure 3B) on k_{cat} for isomerization of GAP (32) by the loss of the single backbone hydrogen bond (Gly-171) between the phosphodianion and loop 6. We suggest that these catalytic elements act cooperatively to stabilize the transition state for substrate deprotonation, so that the elimination of a single element by the LDM or K12G mutation leads to a partial or full loss of the transition state stabilization from the second element.

Figure 4A shows a view from the protein interior of the interaction between the side chain of K12 and the phosphodianion of DHAP (54). The alkylammonium cation lies roughly equidistant from the phosphodianion and carbonyl groups of bound DHAP and interacts with both centers. On moving from the Michaelis complex to the enediolate-like transition state for deprotonation of GAP there is a change in the formal charge at the substrate carbonyl oxygen, from 0 to −1, and in the total charge at bound ligand, from −2 to −3. This increase in charge will result in an increase in the stabilizing electrostatic interactions between the alkylammonium side chain of Lys-12 and the transition state - it was proposed to account for the *ca* 10^4-fold effect of this mutation on k_{cat} for isomerization of GAP (51). An important effect of closure of loop 6 is the partial desolvation of the enzyme active site (31). This results in a reduction in the local dielectric constant of the active site that will lead to a strengthening in the stabilizing interactions between polar side chains and transition state (55). A tightening of polar interactions, including the ion pairing interaction to the side chain of K12, that is the result of loop closure will increase the driving force for closure. This global effect of loop closure on electrostatic and hydrogen bonding interactions may be the reason why the 7 kcal/mol effect of the LDM on the stability of the transition state for

isomerization is so much greater than that any reasonable estimate of the strength of the single loop-dianion interaction eliminated by the LDM (32).

Chemical Reaction Mechanism

Questions continue to be raised about the elegant chemical mechanism for TIM (Figure 1) proposed by Knowles and coworkers (14, 15). Balaram et *al.* have proposed that the side chain of K12 rather than H95 functions to protonate O-2 of DHAP by a mechanism that "*eliminates the need to invoke the formation of the energetically unfavourable imidazolate anion at H95*" (56). We note the following observations that strongly support the mechanism of Knowles and coworkers (Figure 1), where the imidazole side chain of H95 functions as an electrophile in the stabilization of negative charge at isomeric enediolate phosphate intermediates.

1. Formation of imidazolate anion at H95 is not strongly *energetically unfavorable*! The pK_a ≈14 (57) for deprotonation of neutral imidazole in water is marginally higher than pK_a ≈10 for a simple alkylammonium cation; however, the architecture of the active site of TIM favors a reversal in these relative pK_as. The pK_a ≈14 for the neutral side chain of imidazole should be decreased at the protein because of an interaction with the positive end of a short α-helix that stabilizes the imidazole anion (15, 58), and the pK_a ≈10 for the ammonium cation is increased due to stabilization of this cation by ion-pairing to the carboxylate side chain of Glu-97.
2. Protonation of carboxylate side chain of E97, a step in the mechanism proposed by Balaram and coworkers, should not lie on the catalytic cycle for TIM. The X-ray crystal structure of E97Q mutant TIM shows dramatic movement of the K12 side chain away from substrate (56). This is one consequence of the loss of the ion pair between the of K12 and E97 (Figure 4A) and contributes to the large 4000-fold decrease in k_{cat} for E97Q TIM-catalyzed isomerization of GAP (56). The neutral E97 side chain of wildtype TIM, -$CH_2CH_2C(O)OH$, resembles the neutral -$CH_2CH_2C(O)NH_2$ side chain of the E97Q mutant. The conversion of the wildtype side chain anion to the neutral form should therefore cause a conformational change and falloff in catalytic activity similar to that observed for E97Q mutant TIM.
3. An atomic level X-ray crystal structure (0.82 Å resolution) of the enzyme•PGH complex for TIM from *L. mexicana* shows that the hydroxamate oxygens form a bifurcated hydrogen bond to the –N-H of H95 (Figure 4B). This structure of an enediolate analog complex strongly implicates H95 in the stabilization of negative charge at both O-1 and O-2 of the isomeric enediolate phosphate oxyanions intermediates generated by deprotonation of GAP and DHAP respectively (Figure 2), and in mediating proton transfers between these oxygen atoms.

X-ray crystal structures of TIM show an ion pair between the side chains of K12 and E97 (Figure 4A). One role for this ion pair is to immobilize the side chain of K12. This minimizes the decrease in entropy due to the loss of local translational and internal rotational motions that would occur if a flexible side chain were to form an ion pair to the transition state for the isomerization reaction (51). The formation of ion pairs between the anionic side chain of E97 and exogenous ammonium cations at K12G mutant yeast TIM is probably critical to the ability of these cations to *rescue* a substantial portion of the activity of the wildtype enzyme (53).

Phosphite activation

If Eyring transition state theory holds for the reactions of small molecules in water and at enzyme active sites, then the underlying cause of enzymatic catalysis is the stabilization of

the transition state by strong "binding" interactions with the protein catalyst (59). This total transition state stabilization is often so large that it cannot be expressed entirely at the Michaelis complex, because this would result in effectively irreversible ligand binding and strongly rate determining product release (60). Enzymes therefore show specificity in binding their transition states with higher affinity than substrate. We consider now the molecular explanation for the specificity of TIM towards binding the isomerization transition state.

Between 4 and 5 of the total 12 kcal/mole intrinsic phosphodianion binding energy is expressed as phosphite dianion activation of TIM for catalysis of the reactions of [1-^{13}C]-GA (42, 43). This binding energy cannot be utilized to anchor the carbon acid substrate GA to TIM (K_m effect), and must therefore be specifically expressed at the transition state (k_{cat} effect) for the TIM-catalyzed reactions of GA and, by analogy, at the transition state for TIM-catalyzed reactions of the whole substrates GAP and DHAP.

The large difference between K_d = 38 mM and $K_d^{\dagger} \approx 20$ μM (Scheme 5) for binding of HPO_3^{2-} to free TIM and to E•GA†, respectively, might reflect a direct interaction between the pieces, that stabilizes the ternary complex. However, the anionic enediolate-like transition state for TIM-catalyzed deprotonation of GA (51) should show unfavorable electrostatic interactions with bound phosphite dianion. Scheme 6 presents a mechanism for the activation of TIM by HPO_3^{2-} (42). TIM is proposed to exist in two forms: a dominant inactive loop open enzyme E_O with a low affinity for ligand binding, and a rare active loop-closed enzyme (E_C, $K_c \ll 1$, Scheme 6) that shows specificity in binding to phosphite dianion and to the transition state GA†. The binding of HPO_3^{2-} is weak and the TIM-catalyzed reaction of GA slow, because the concentration of the closed enzyme E_C is low, so that a substantial portion of the ligand binding energy is used to drive the unfavorable conformational change. For example, only 1.9 of the total 6.4 kcal/mol phosphite dianion binding energy is observed upon formation of the Michaelis complex (Figure 5A). Once the energetic price for loop closure is paid, the full intrinsic ligand binding energy is expressed on binding of the second ligand; either HPO_3^{2-} or GA† to form the ternary E•GA†• HPO_3^{2-} complex (Figure 5A).

Scheme 6 assumes that there is a significant difference in the energy of E_O and E_C; and, in the reactivity of these different enzyme forms toward deprotonation of bound substrate. Six water molecules lie within 5 Å of the side chain of the catalytic base Glu-167 at unliganded *Tbb*TIM (61). The closure of loop 6 over bound ligands occludes bulk solvent and displaces several water molecules from the active site. Only two waters lie within 5 Å of the side chain of Glu-167 at the complex between TIM (*L. mexicana*) and PGH (62). The stripping of the polar solvent water from the active site (desolvation) should result in an increase in the energy of E_C compared to E_O.

X-ray crystal structures show that ligand-driven closure of loop 6 results in displacement of the carboxylate side chain of the active site base by several angstroms towards the ligand. The carboxylate oxygen of Glu-165 lies only 3.0 Å from the ketone and α-hydroxy carbons of DHAP at a high resolution (1.2 Å) crystal structure of *c*TIM (54). Preorganization of this basic side chain may facilitate transfer of a hydron from C-1 of DHAP to TIM. This proposal is supported by circumstantial evidence that small shifts in the position of the side chain at mutant forms of TIM are associated with substantial reductions in catalytic activity. For example, a comparison of X-ray crystal structures of *c*TIM-PGH complexes show the carboxylate group of the catalytic base shifted by 0.7 Å (E165D (63)) and 0.4 Å (S96P (64)) from its position in wildtype *c*TIM. The E165D (65) and S96P (66) mutations cause 240-fold and 11-fold decreases, respectively, in k_{cat} for wildtype TIM and a < 2-fold increase in

K_m. It was also proposed that these mutations result in changes in the positioning of waters at the active site that affect catalytic activity (64).

Wierenga's lucid analysis of the changes in protein structure that occur during the ligand-gated loop closure (8) bring to mind a precision mechanical device, such as a Swiss watch. Loop closure drives the hydrophobic side chain of Ile-172 of *Tbb*TIM towards the carboxylate side chain of Glu-167, and this "pushes" the side chain anion toward the second immobile hydrophobic side chain of Leu-232 (Figure 6). This conformational change sandwiches the carboxylate side-chain between two hydrophobic side chains and shields it from interactions with bulk solvent. "Hydrophobic clamping" should lead to an increase in the basicity of the carboxylate anion, and hence in its reactivity toward deprotonation of carbon.

We have probed the role of I172 and L232 in activation of *Tbb*TIM for deprotonation of carbon. The I172A mutations results in a 200-fold decrease in k_{cat} for isomerization of the whole substrate GAP, but only a small <2-fold change in K_m (67). The I172A mutant shows no detectable activity towards deprotonation of [1-^{13}C]-GA: this corresponds to a >10-fold decrease in $(k_{cat}/K_m)_E$ (Scheme 5). The mutation results in a large 300-fold decrease in $(k_{cat}/K_m)_{E•Pi}$, but there is little change in K_d for binding of phosphite dianion compared with wildtype *Tbb*TIM (67). These results show that the hydrophobic side chain of I172A plays no role in the stabilization of the Michaelis complex to GAP or phosphite dianion, and a significant role in effecting the stabilization of the transition states for the wildtype TIM-catalyzed reactions of GAP and the substrate pieces. They provide support for the proposal that the "hydrophobic clamping" that accompanies loop closure (68) has the effect of enhancing the reactivity of the side chain of Glu-167 towards deprotonation of bound substrates (Figure 6).

The side chain of L232, which is contained in loop 8, remains nearly fixed during loop closure. The L232A mutation causes a small 6-fold decrease in k_{cat}/K_m for the *Tbb*TIM-catalyzed isomerization of GAP to give DHAP. We were surprised to observe that this mutation leads to an *increase* in the enzymatic activity toward catalysis of the reaction of the substrate pieces (69). There is a 17-fold *increase* and 16-fold *decrease* compared to wildtype TIM, respectively, in $(k_{cat}/K_m)_E$ for deprotonation of [1-^{13}C]-GA and in the dissociation constant K_d for HPO_3^{2-} (Scheme 5). On the other hand, similar values of $(k_{cat}/K_m)_{E•Pi}$ are observed for the wildtype and L232A mutant enzymes (69). The net effect of the L232A mutation is therefore to enhance the activity of free enzyme, but not the activity of the E•P_i complex, towards deprotonation of [1-^{13}C]-GA. The result is a *larger* activation of the wildtype compared to L232A mutant enzyme-catalyzed reactions by the binding of HPO_3^{2-}.

The critical observation of a 17-fold *increase* in $(k_{cat}/K_m)_E$ for the [supposedly crippled] L232A mutant enzyme-catalyzed reaction of [1-^{13}C]-GA is in keeping with our proposal that a portion of the ligand binding energy for wildtype TIM is *wasted* in driving an unfavorable conformational change. The higher activity for L232A mutant TIM can be rationalized by a decrease in the barrier to this conformational change [increase in K_C, Scheme 6], in which case a larger fraction of the ligand binding energy will be observed as stabilization of the transition state for the L232A mutant TIM-catalyzed reaction of [1-^{13}C]-GA. Specifically, the L232A mutation is proposed to cause a *ca* 17-fold increase in K_c for the thermodynamically unfavorable conversion of an inactive loop open form of TIM (E_O) to a higher energy, but active, loop closed enzyme (E_c), which corresponds to a 1.7 kcal/mol change in ΔG_c.

Figure 5B illustrates the effect of a decrease in ΔG_c on the kinetic parameters for the TIM-catalyzed reactions of the substrate pieces. The proposed barrier to conversion of E_O to E_C

(ΔG_c = 4.5 kcal/mol) for wildtype *Tbb*TIM is given by the SUM of the red and black bars in the lower left hand corner of Figure 5B. The red bars show the magnitude of the effect of the L232A mutation on this barrier, $\Delta\Delta G_c \approx 1.7$ kcal/mol. The barrier to ΔG_c is included in the barriers to formation of both the binary and ternary complexes (Figure 5B). Therefore, a decrease in ΔG_c would result in an increase in $(k_{cat}/K_m)_E$ (17-fold) a decrease in K_d (16-fold) and an increase in $(k_{cat}/K_m)_E/K_d$ (25-fold). The magnitude of the activation of TIM for deprotonation of GA by the binding of phosphite dianion is determined by the magnitude of ΔG_c, and will therefore decrease.

Figures 5A and 5B provide a framework for interpreting the effect of the L232A mutation on the kinetic parameters for the TIM-catalyzed reactions of whole and truncated substrates. However, this model needs to be expanded and refined and there is of course the need for additional experimental work. For example:

1. The model predicts that an increase in K_c results in an increase in the kinetic parameters for the substrate pieces that react specifically with the closed enzyme E_C. However, this change cannot cause an increase in k_{cat}/K_m for isomerization of the whole substrate GAP, because this reaction is already diffusion limited (70). The small six-fold decrease in k_{cat}/K_m for isomerization of the whole substrate GAP by the L232A mutant cannot be rationalized by an increase in $[E_C]$ relative to $[E_O]$. This effect might reflect small shifts in the position of the active site catalytic residues at the L232A mutant that lead to a *decrease* in the stabilization of the transition state for the reaction of the whole substrate GAP or DHAP, but not for the reaction of $[GA + HPO_3^{2-}]$, because cutting the covalent connection allows for independent movement of the pieces to their most reactive conformations at the active site.

2. We envisioned similar functions for the hydrophobic side chains of I172 and L232 in desolvation of the basic side chain of E167, and in clamping this side chain next to the carbon acid substrate. However, mutations of I172 and L232 result in different changes in kinetic parameters. The I172A substitution causes a decrease in the reactivity of TIM for deprotonation of the whole substrate and the substrate pieces (67). Apparently the interactions between the mobile side chains of E167 and I172 function to activate TIM for deprotonation of bound substrate. The L232A substitution causes a surprising *increase* in the kinetic parameter for catalysis of deprotonation of GA. Now, unfavorable interactions between E167 and the fixed side chain of L232 that develop upon loop closure are suggested to destabilize E_C, so that stabilization of E_C by interaction with phosphite dianion activates TIM for catalysis.

3. It is important to consider the evolutionary force(s) that might select for a catalyst that exists predominately as a form that is inactive (E_O, Scheme 6). We suggest that this is partly or entirely due to the requirement that enzyme active sites be solvent-exposed in order to allow for substrate binding, and the catalytic advantages [see above] that arise from thermodynamically unfavorable active site desolvation during conversion of E_O to E_C. Note that the requirement for an unfavorable conformational change will not affect k_{cat}/K_m for turnover of GAP, so long as the substrate reaction remains diffusion limited. This is the case when the chemical steps are fast; and, loop closure over GAP is thermodynamically favorable and faster than release of substrate to water. The phosphite dianion binding energy that is utilized to drive the conversion of E_O to E_C is not expressed at the Michaelis complex. This is required in order to avoid very tight ligand binding, and strongly rate determining product release (60).

Concluding Remarks

The focus of classical kinetic studies of enzyme-catalyzed reactions is the determination of various kinetic parameters that define the relative stability of the free enzyme, Michaelis complexes, and the reaction transition state. These studies do not provide information about the changes in protein structure that occur on proceeding first to the Michaelis complex and then to the transition state. These changes need to be considered when interpreting kinetic data; for example, the large conformational changes of TIM observed upon ligand binding. It is unclear whether the rate acceleration for TIM is enhanced by any requirement for the coupling of these protein motions to the chemical steps for the catalyzed reaction (71, 72). However, at our modest empirical level, the rate acceleration of TIM-catalyzed isomerization can be accounted for by a consideration of the stabilizing interactions between the protein catalyst and transition state for deprotonation of α–carbonyl carbon.

References

1. Hayden EC. Chemistry: Designer debacle. Nature (London, U K). 2008; 453:275–278.
2. Rieder SV, Rose IA. Mechanism of the triose phosphate isomerase reaction. J Biol Chem. 1959; 234:1007–1010. [PubMed: 13654309]
3. Shonk CE, Boxer GE. Enzyme patterns in human tissues. I. Methods for the determination of glycolytic enzymes. Can Res. 1964; 24:709–721.
4. Webster KA. Evolution of the coordinate regulation of glycolytic enzyme genes by hypoxia. J Exp Biol. 2003; 206:2911–2922. [PubMed: 12878660]
5. Richard JP, Amyes TL. Proton transfer at carbon. Curr Op Chem Biol. 2001; 5:626–633.
6. Gerlt JA, Kozarich JW, Kenyon GL, Gassman PG. Electrophilic Catalysis Can Explain the Unexpected Acidity of Carbon Acids in Enzyme-Catalyzed Reactions. J Am Chem Soc. 1991; 113:9667–9669.
7. Knowles JR, Albery WJ. Perfection in enzyme catalysis: the energetics of triosephosphate isomerase. Acc Chem Res. 1977; 10:105–111.
8. Wierenga RK. Triosephosphate isomerase: a highly evolved biocatalyst. Cell Mol Life Sci. 2010; 67:3961–3982. [PubMed: 20694739]
9. Miller JC, Waley SG. Active center of rabbit muscle triose phosphate isomerase. Site that is labeled by glycidol phosphate. Biochem J. 1971; 123:163–170. [PubMed: 4942534]
10. Waley SG, Miller JC, Rose IA, O'Connell EL. Identification of site in triose phosphate isomerase labeled by glycidol phosphate. Nature. 1970; 227:181. [PubMed: 5428408]
11. Nickbarg EB, Davenport RC, Petsko GA, Knowles JR. Triosephosphate isomerase: removal of a putatively electrophilic histidine residue results in a subtle change in catalytic mechanism. Biochemistry. 1988; 27:5948–5960. [PubMed: 2847777]
12. Lodi PJ, Chang LC, Knowles JR, Komives EA. Triosephosphate isomerase requires a positively charged active site: The role of lysine-12. Biochemistry. 1994; 33:2809–2814. [PubMed: 8130193]
13. Joseph-McCarthy D, Lolis E, Komives EA, Petsko GA. Crystal structure of the K12M/G15A triosephosphate isomerase double mutant and electrostatic analysis of the active site. Biochemistry. 1994; 33:2815–2823. [PubMed: 8130194]
14. Knowles JR. Enzyme catalysis: not different, just better. Nature. 1991; 350:121–124. [PubMed: 2005961]
15. Knowles JR. To build an enzyme. Philos Trans R Soc London, Ser B. 1991; 332:115–121. [PubMed: 1678530]
16. Richard JP. Acid-base catalysis of the elimination and isomerization reactions of triose phosphates. J Am Chem Soc. 1984; 106:4926–4936.
17. Amyes TL, Richard JP. Generation and stability of a simple thiol ester enolate in aqueous solution. J Am Chem Soc. 1992; 114:10297–10302.

18. Amyes TL, Richard JP. Determination of the pK_a of ethyl acetate: Brønsted correlation for deprotonation of a simple oxygen ester in aqueous solution. J Am Chem Soc. 1996; 118:3129–3141.
19. Richard JP, Williams G, Gao JL. Experimental and computational determination of the effect of the cyano group on carbon acidity in water. J Am Chem Soc. 1999; 121:715–726.
20. Rios A, Amyes TL, Richard JP. Formation and stability of organic zwitterions in aqueous solution: Enolates of the amino acid glycine and its derivatives. J Am Chem Soc. 2000; 122:9373–9385.
21. Chaing Y, Guo H-X, Kresge AJ, Richard JP, Toth K. The Mandelamid Keto-Enol System in Aqueous Solution. Generation of the Enol by Hydration of Phenylcarbamoylcarbene. J Am Chem Soc. 2002; 125:187–194.
22. Richard JP, Williams G, O'Donoghue AC, Amyes TL. Formation and stability of enolates of acetamide and acetate anion: An Eigen plot for proton transfer at α-carbonyl carbon. J Am Chem Soc. 2002; 124:2957–2968. [PubMed: 11902887]
23. O'Donoghue AC, Amyes TL, Richard JP. Hydron Transfer Catalyzed by Triosephosphate Isomerase. Products of Isomerization of (R)-Glyceraldehyde 3-Phosphate in D_2O. Biochemistry. 2005; 44:2610–2621. [PubMed: 15709774]
24. O'Donoghue AC, Amyes TL, Richard JP. Hydron Transfer Catalyzed by Triosephosphate Isomerase. Products of Isomerization of Dihydroxyacetone Phosphate in D_2O. Biochemistry. 2005; 44:2622–2631. [PubMed: 15709775]
25. Fisher LM, Albery WJ, Knowles JR. Energetics of triosephosphate isomerase: the nature of the proton transfer between the catalytic base and solvent water. Biochemistry. 1976; 15:5621–5626. [PubMed: 999837]
26. Eigen M. Proton Transfer, Acid-Base Catalysis, and Enzymatic Hydrolysis. Angew Chem Int Ed Engl. 1964; 3:1–72.
27. Tu C, Paranawithana SR, Jewell DA, Tanhauser SM, LoGrasso PV, Wynns GC, Laipis PJ, Silverman DN. Buffer Enhancement of Proton Transfer in Catalysis by Human Carbonic Anhydrase III. Biochemistry. 1990; 29:6400–6405. [PubMed: 2169869]
28. O'Donoghue AC, Amyes TL, Richard JP. Slow proton transfer from the hydrogen-labelled carboxylic acid side chain (Glu-165) of triosephosphate isomerase to imidazole buffer in D_2O. Org Biomol Chem. 2008; 6:391–396. [PubMed: 18175010]
29. Rose IA, Fung WJ, Warms JVB. Proton diffusion in the active site of triosephosphate isomerase. Biochemistry. 1990; 29:4312–4317. [PubMed: 2161683]
30. Albery WJ, Knowles JR. Free-energy profile for the reaction catalyzed by triosephosphate isomerase. Biochemistry. 1976; 15:5627–5631. [PubMed: 999838]
31. Malabanan MM, Amyes TL, Richard JP. A role for flexible loops in enzyme catalysis. Curr Op Struct Biol. 2010; 20:702–710.
32. Pompliano DL, Peyman A, Knowles JR. Stabilization of a reaction intermediate as a catalytic device: definition of the functional role of the flexible loop in triosephosphate isomerase. Biochemistry. 1990; 29:3186–3194. [PubMed: 2185832]
33. Berlow RB, Igumenova TI, Loria JP. Value of a Hydrogen Bond in Triosephosphate Isomerase Loop Motion. Biochemistry. 2007; 46:6001–6010. [PubMed: 17455914]
34. Guthrie JP, Kluger R. Electrostatic Stabilization Can Explain the Unexpected Acidity of Carbon Acids in Enzyme-Catalyzed Reactions. J Am Chem Soc. 1993; 115:11569–11572.
35. Richard JP, Amyes TL. On the importance of being zwitterionic: enzymic catalysis of decarboxylation and deprotonation of cationic carbon. Bioorg Chem. 2004; 32:354–366. [PubMed: 15381401]
36. Harris TK, Abeygunawardana C, Mildvan AS. NMR studies of the role of hydrogen bonding in the mechanism of triosephosphate isomerase. Biochemistry. 1997; 36:14661–14675. [PubMed: 9398185]
37. Cleland WW, Frey PA, Gerlt JA. The Low Barrier Hydrogen Bond in Enzymatic Catalysis. J Biol Chem. 1998; 273:25529–25532. [PubMed: 9748211]
38. Wolfenden R. Enzyme catalysis. Conflicting requirements of substrate access and transition state affinity. Mol Cell Biochem. 1974; 3:207–211. [PubMed: 4365214]

39. Putman SJ, Coulson AFW, Farley IRT, Riddleston B, Knowles JR. Specificity and kinetics of triose phosphate isomerase from chicken muscle. Biochem J. 1972; 129:301–310. [PubMed: 4643318]
40. Amyes TL, O'Donoghue AC, Richard JP. Contribution of phosphate intrinsic binding energy to the enzymatic rate acceleration for triosephosphate isomerase. J Am Chem Soc. 2001; 123:11325–11326. [PubMed: 11697989]
41. Go MK, Amyes TL, Richard JP. Hydron Transfer Catalyzed by Triosephosphate Isomerase. Products of the Direct and Phosphite-Activated Isomerization of [1-^{13}C]-Glycolaldehyde in D_2O. Biochemistry. 2009; 48:5769–5778. [PubMed: 19425580]
42. Amyes TL, Richard JP. Enzymatic catalysis of proton transfer at carbon: Activation of triosephosphate isomerase by phosphite dianion. Biochemistry. 2007; 46:5841–5854. [PubMed: 17444661]
43. Malabanan MM, Go M, Amyes TL, Richard JP. Wildtype and Engineered Monomeric Triosephosphate Isomerase from Trypanosoma brucei: Partitioning of Reaction Intermediates in D_2O and Activation by Phosphite Dianion. Biochemistry. 2011; 50:5767–5679. [PubMed: 21553855]
44. Jencks WP. On the attribution and additivity of binding energies. Proc Natl Acad Sci. 1981; 78:4046–4050. [PubMed: 16593049]
45. Page MI, Jencks WP. Entropic contributions to rate accelerations in enzymic and intramolecular reactions and the chelate effect. Proc Natl Acad Sci. 1971; 68:1678–1683. [PubMed: 5288752]
46. Borchert TV, Abagyan R, Jaenicke R, Wierenga RK. Design, creation, and characterization of a stable, monomeric triosephosphate isomerase. Proc Natl Acad Sci. 1994; 91:1515–1518. [PubMed: 8108439]
47. Toteva MM, Silvaggi NR, Allen KN, Richard JP. Binding Energy and Catalysis by D-Xylose Isomerase: Kinetic, Product, and X-ray Crystallographic Analysis of Enzyme-Catalyzed Isomerization of (R)-Glyceraldehyde. Biochemistry. 2011; 50:10170–10181. [PubMed: 21995300]
48. Amyes TL, Richard JP, Tait JJ. Activation of orotidine 5′-monophosphate decarboxylase by phosphite dianion: The whole substrate is the sum of two parts. J Am Chem Soc. 2005; 127:15708–15709. [PubMed: 16277505]
49. Tsang WY, Amyes TL, Richard JP. A substrate in pieces: Allosteric activation of glycerol 3-phosphate dehydrogenase (NAD^+) by phosphite dianion. Biochemistry. 2008; 47:4575–4582. [PubMed: 18376850]
50. Zhang Z, Sugio S, Komives EA, Liu KD, Knowles JR, Petsko GA, Ringe D. Crystal Structure of Recombinant Chicken Triosephosphate Isomerase-Phosphoglycolohydroxamate Complex at 1.8-Å Resolution. Biochemistry. 1994; 33:2830–2837. [PubMed: 8130195]
51. Go MK, Koudelka A, Amyes TL, Richard JP. Role of Lys-12 in Catalysis by Triosephosphate Isomerase: A Two-Part Substrate Approach. Biochemistry. 2010; 49:5377–5389. [PubMed: 20481463]
52. Richard JP. Kinetic-parameters for the elimination reaction catalyzed by triosephosphate isomerase and an estimation of the reactions physiological significance. Biochemistry. 1991; 30:4581–4585. [PubMed: 2021650]
53. Go MK, Amyes TL, Richard JP. Rescue of K12G mutant TIM by NH_4^+ and alkylammonium cations: The reaction of an enzyme in pieces. J Am Chem Soc. 2010; 132:13525–13532. [PubMed: 20822141]
54. Jogl G, Rozovsky S, McDermott AE, Tong L. Optimal alignment for enzymatic proton transfer: structure of the Michaelis complex of triosephosphate isomerase at 1.2-Å resolution. Proc Natl Acad Sci. 2003; 100:50–55. [PubMed: 12509510]
55. Hine, J. Structural Effects on Equilibria in Organic Chemistry. Wiley-Interscience; New York: 1975.
56. Samanta M, Murthy MRN, Balaram H, Balaram P. Revisiting the Mechanism of the Triosephosphate Isomerase Reaction: The Role of the Fully Conserved Glutamic Acid 97 Residue. Chembiochem. 2011; 12:1886–1895. [PubMed: 21671330]
57. Yagil G. Proton Dissociation Constant of Pyrrole Indole and Related Compounds. Tetrahedron. 1967; 23:2855. [PubMed: 6047529]

58. Komives EA, Chang LC, Lolis E, Tilton RF, Petsko GA, Knowles JR. Electrophilic catalysis in triosephosphate isomerase: the role of histidine-95. Biochemistry. 1991; 30:3011–3019. [PubMed: 2007138]
59. Pauling L. Nature of forces between large molecules of biological interest. Nature. 1948; 161:707–709. [PubMed: 18860270]
60. Jencks WP. Binding energy, specificity and enzymic catalysis: The Circe effect. Adv Enzymology Relat Areas Mol Biol. 1975; 43:219–410.
61. Wierenga RK, Noble MEM, Vriend G, Nauche S, Hol WGJ. Refined 1.83 Å structure of trypanosomal triosephosphate isomerase crystallized in the presence of 2.4 M-ammonium sulfate. A comparison with the structure of the trypanosomal triosephosphate isomerase-glycerol-3-phosphate complex. J Mol Biol. 1991; 220:995–1015. [PubMed: 1880808]
62. Alahuhta M, Wierenga RK. Atomic Resolution crystallography of a complex of triosephosphate isomerase with a reaction intermediate analog: new insight in the proton transfer reaction mechanism. Proteins: Structure, Function and Bioinformatics. 2010; 78:1878–1888.
63. Joseph-McCarthy D, Rost LE, Komives EA, Petsko GA. Crystal Structure of the Mutant Yeast Triosephosphate Isomerase in Which the Catalytic Base Glutamic Acid 165 Is Changed to Aspartic Acid. Biochemistry. 1994; 33:2824–2829. [PubMed: 7907502]
64. Zhang Z, Komives EA, Sugio S, Blacklow SC, Narayana N, Xuong NH, Stock AM, Petsko GA, Ringe D. The Role of Water in the Catalytic Efficiency of Triosephosphate Isomerase. Biochemistry. 1999; 38:4389–4397. [PubMed: 10194358]
65. Straus D, Raines R, Kawashima E, Knowles JR, Gilbert W. Active site of triosephosphate isomerase: in vitro mutagenesis and characterization of an altered enzyme. Proc Natl Acad Sci. 1985; 82:2272–2276. [PubMed: 3887397]
66. Blacklow SC, Knowles JR. How can a catalytic lesion be offset? The energetics of two pseudorevertant triosephosphate isomerases. Biochemistry. 1990; 29:4099–4108. [PubMed: 2361134]
67. Malabanan MM. Unpublished results.
68. Kursula I, Wierenga RK. Crystal structure of triosephosphate isomerase complexed with 2-phosphoglycolate at 0.83-Å resolution. J Biol Chem. 2003; 278:9544–9551. [PubMed: 12522213]
69. Malabanan MM, Amyes TL, Richard JP. Mechanism for Activation of Triosephosphate Isomerase by Phosphite Dianion: The Role of a Ligand-Driven Conformational Change. J Am Chem Soc. 2011; 133:16428–16431. [PubMed: 21939233]
70. Blacklow SC, Raines RT, Lim WA, Zamore PD, Knowles JR. Triosephosphate isomerase catalysis is diffusion controlled. Biochemistry. 1988; 27:1158–1165. [PubMed: 3365378]
71. Olsson MHM, Parson WW, Warshel A. Dyanamical contributions to enzyme catalysis: Critical tests of a popular hypothesis. Chem Rev. 2006; 106:1737–1756. [PubMed: 16683752]
72. Nagel ZD, Klinman JP. A 21st century revisionists' view at a turning point in enzymology. Nat Chem Biol. 2009; 8:543–550. [PubMed: 19620995]
73. Lolis E, Petsko GA. Crystallographic analysis of the complex between triosephosphate isomerase and 2-phosphoglycolate at 2.5-Å resolution: implications for catalysis. Biochemistry. 1990; 29:6619–6625. [PubMed: 2204418]

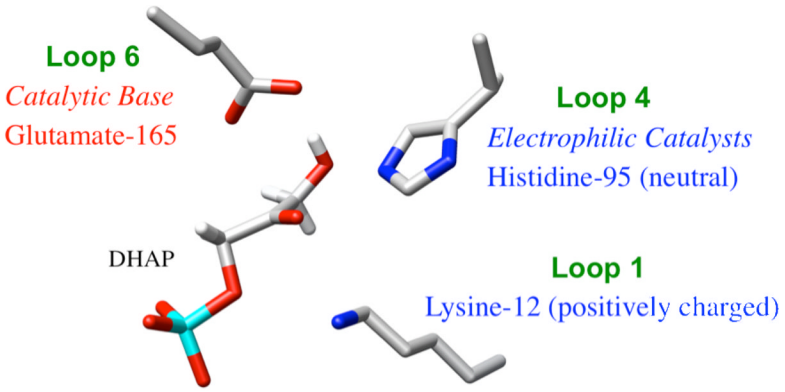

Figure 1.
The orientation of the catalytic side chains at the active site of TIM [PDB entry 1NEY] (54). The carboxylate side chain of E165 found at the front of flexible loop 6 is positioned to deprotonate the carbon acid substrate of DHAP. The neutral imidazole side chain of H95, which is part of loop 4, is positioned to form hydrogen bonds to O-1 or O-2 of isomeric enediolate phosphate reaction intermediates. The cationic side chain of K12, which is part of loop 1, forms an ion pair to the phosphodianion of substrate.

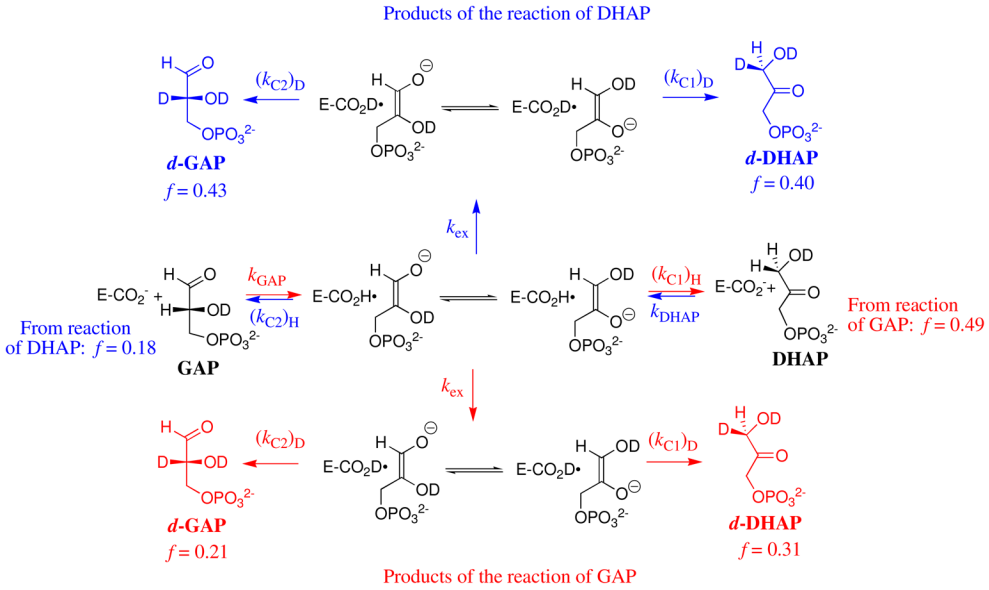

Figure 2.

The pathways for formation of the products of the TIM-catalyzed reactions of GAP and DHAP in D_2O. The yields of the products of the reaction of GAP are shown in red and the yields of the products of the reaction of DHAP are shown in blue.

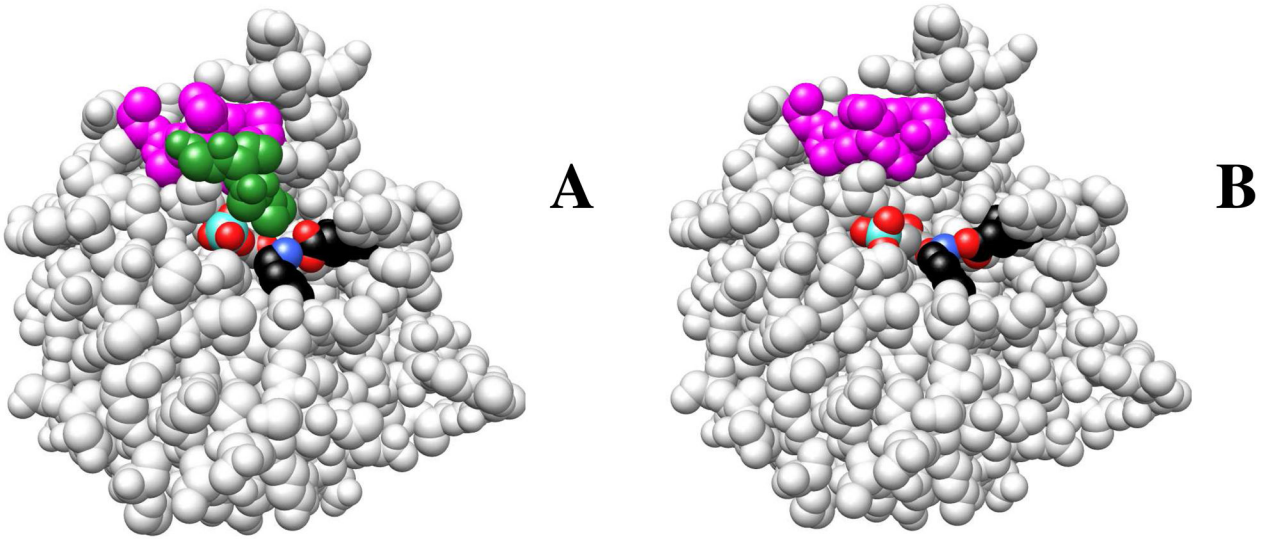

Figure 3.

(A) Space filling model of the complex between TIM from yeast and PGA [PDB entry 2YPI] (73). The amino acid side chains of loop 6 that were kept for the LDM are shaded magenta, and the deleted residues are shaded green. The cationic side chain of K12 is shown on the left hand side of the protein with the nitrogen (blue) in an ion pair to oxygen (red) of the anionic side chain of E97. (B) The LDM of TIM generated from the structure for wildtype TIM (Figure 3A) by a procedure similar to that described for the K12G mutant of TIM from yeast (53). The amino acid side chains of loop 6 that were preserved for the LDM are shaded magenta.

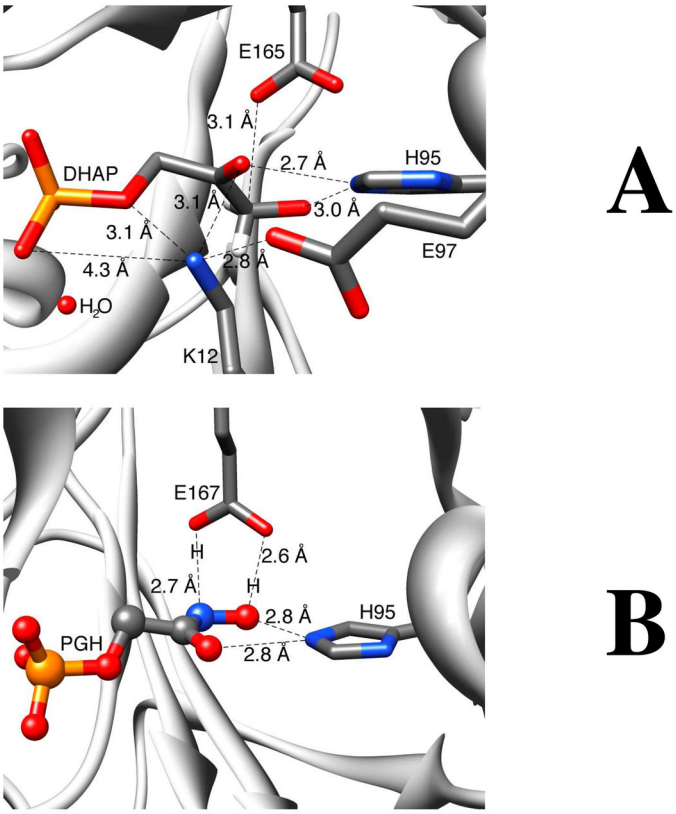

Figure 4.

(A) The active site of TIM, taken from the X-ray crystal structure of McDermott and coworkers (PDB entry 1NEY) (54), showing the distances between the ammonium nitrogen of Lys-12 and the functional groups of bound substrate DHAP. (B) The 0.82 Å resolution structure of the complex between TIM (*L. mexicana*) and the enediolate intermediate analog PGH [PDB entry 2VXN] (62) showing the distances from the catalytic side chains to the ligand.

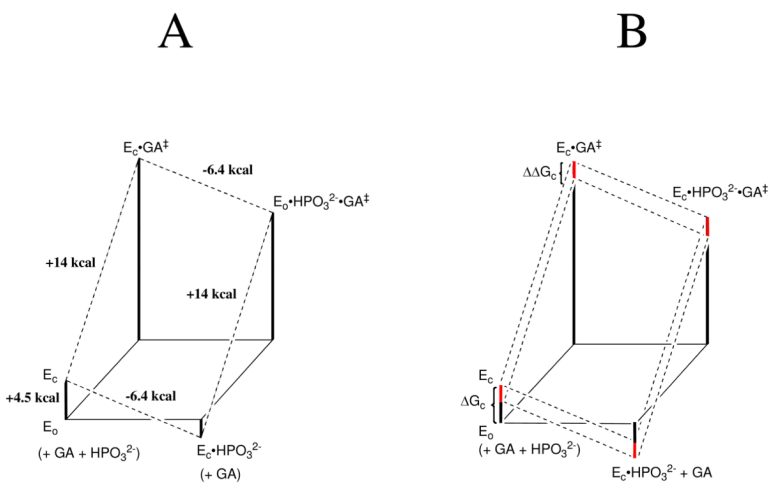

Figure 5.

(A) Free energy profile for turnover of GA by free TIM (E_O) and by TIM that is saturated with phosphite dianion (E_C•HPO_3^{2-}) that shows activation free energy changes calculated using the Eyring equation at 298 K. The difference between the total intrinsic phosphite binding energy of −6.4 kcal/mol and ΔG^o = −1.9 kcal/mol for binding of HPO_3^{2-} to the inactive open ground state enzyme E_O to give the active closed liganded enzyme E_C•HPO_3^{2-} is attributed to ΔG_C = 4.5 kcal/mol for an unfavorable conformational change that converts E_O to E_C. The observed value of $\Delta G^{\ddagger}$ = +18.5 kcal/mol for turnover of GA may be partitioned conceptually into $\Delta G^{\ddagger}$ = +14 kcal/mol for proton transfer catalyzed by E_C and ΔG_C = 4.5 kcal/mol for the obligate conformational change that converts E_O to E_C. (B) Free energy profile that shows the effect of the L232A mutation on the kinetic parameters for wildtype *Tbb*TIM catalyzed reactions of the substrate pieces. The red bars show the proposed effect of the L232A mutation on the barrier for the conformational change from E_O to E_C ($\Delta\Delta G_C$). The effect of this change in ΔG_C on turnover of the substrate pieces is shown by a comparison of the reaction profiles for wildtype TIM (upper dashed lines) and L232A mutant TIM (lower dashed lines).

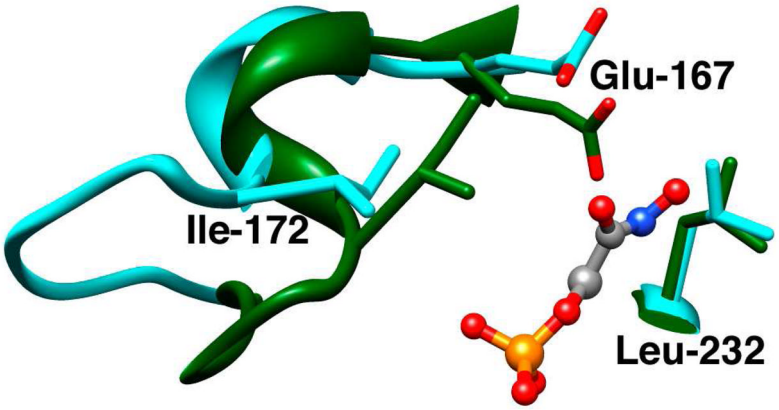

Figure 6.

Superposition of models, from X-ray crystal structures, of the unliganded open (cyan, PDB entry 5TIM) and the PGH-liganded closed (green, PDB entry 1TRD) forms of *Tbb*TIM in the region of the enzyme active site. Closure of loop 6 (residues 168 – 178) over the ligand phosphodianion group shifts the hydrophobic side chain of Ile-172 towards the carboxylate side chain of the catalytic base Glu-167. This is accompanied by movement of Glu-167 towards the hydrophobic side chain of Leu-232, which maintains a nearly fixed position.

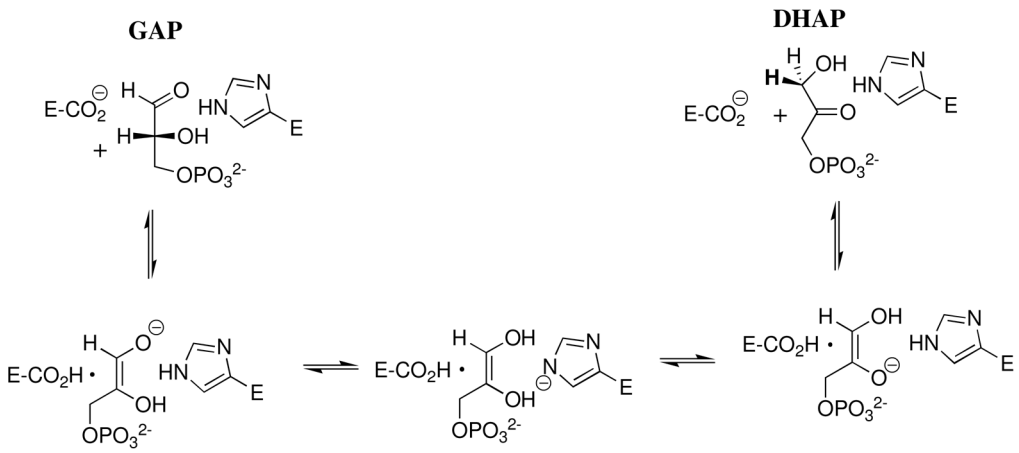

Scheme 1.

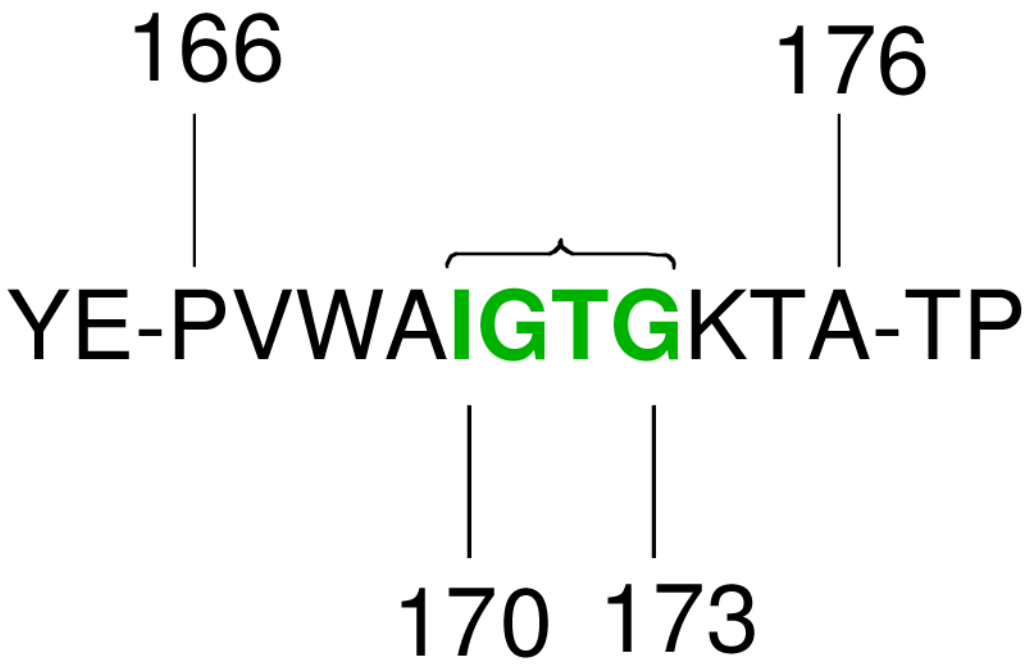

Scheme 2.

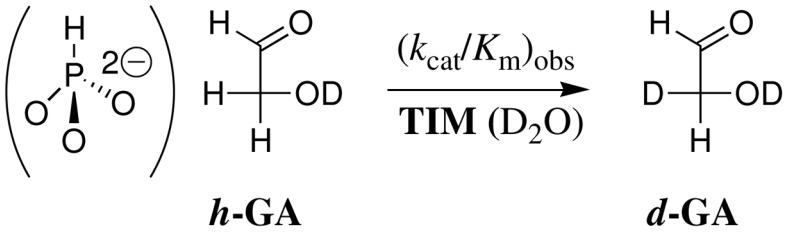

***h*-GA** ***d*-GA**

Scheme 3.

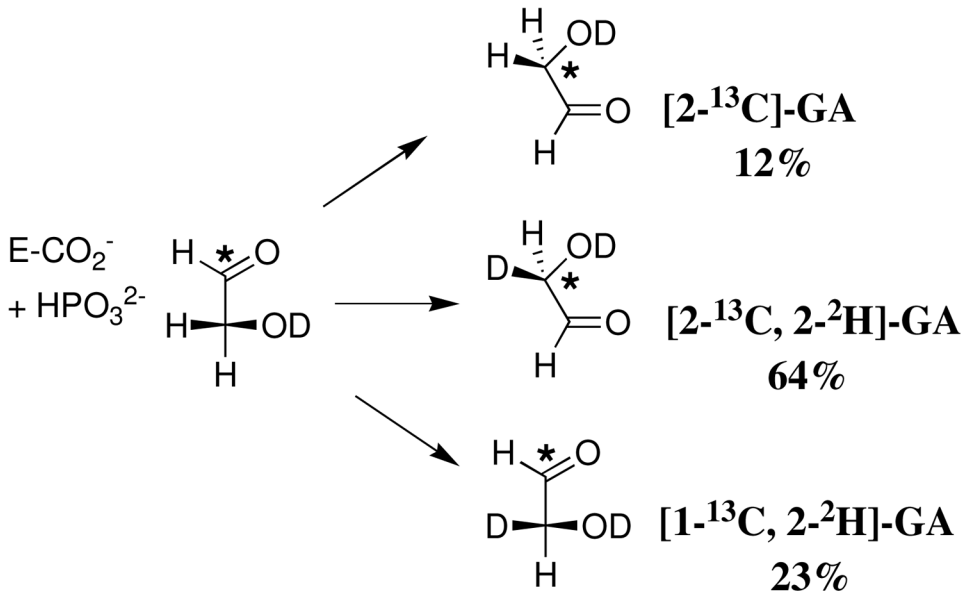

Scheme 4.

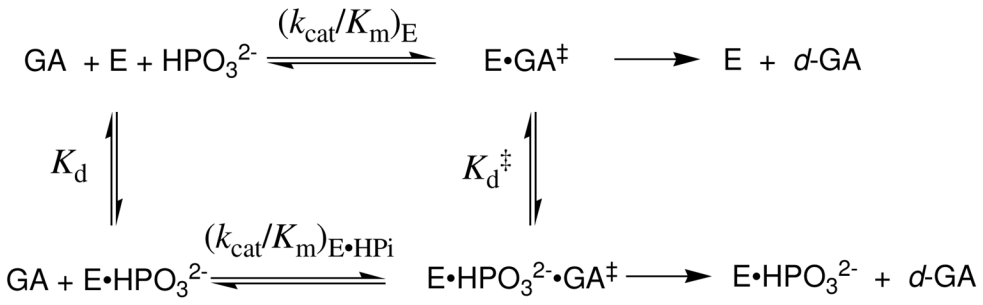

Scheme 5.

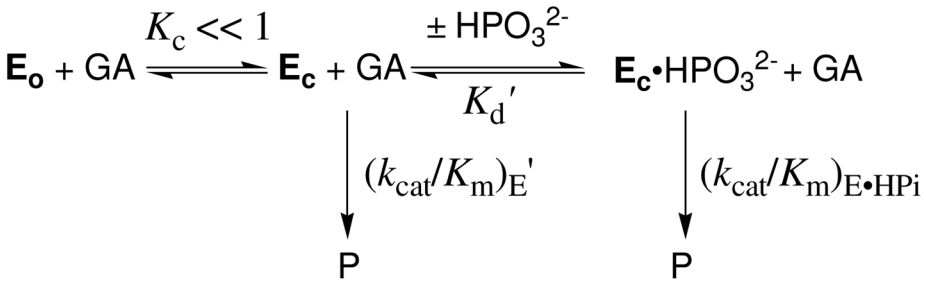

Scheme 6.